

www.acsanm.org Article

Adaptive Cavitation Ultrasonication for Large-Scale Preparation of Porous Silicon Nanoparticles

Jaehui Lee, Hye Ji Um, Michael J. Sailor,* Jaehoon Kim,* Hwajun Jeong,* and Dokyoung Kim*



Cite This: https://doi.org/10.1021/acsanm.4c00908



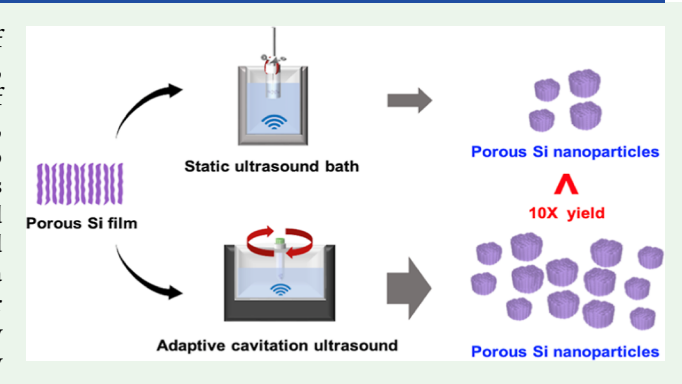
ACCESS

III Metrics & More

Article Recommendations

Supporting Information

ABSTRACT: Porous silicon nanoparticles (pSiNPs) are of increased interest for use in drug delivery systems, as catalysts, and as biomedical imaging agents. The most common synthesis of pSiNPs involves electrochemical anodization of a silicon wafer, followed by ultrasonic fracture of the resulting mesoporous film to form well-defined nanoparticles. A major source of loss in this process is the ultrasonic fracture step. This work presents a method of synthesizing gram-scale quantities of pSiNPs with high yield and high reproducibility using an ultrasonic bath equipped with a sample rotation stage and a refrigerator (4 °C) and a higher ultrasound frequency with power delivered in a pulsed modality compared with the static ultrasound "cleaning baths" commonly used for this purpose. The optimal processing conditions are



determined by adjusting the pSi film mass, solvent volume, and iteration number of on/off cycles used in sonication. The approach provides pSiNPs with a narrow size distribution (\sim 170 nm, PDI = 0.149), higher yields (59%), and an approximately 12-fold reduction in the total processing time, allowing the preparation of gram-scale quantities of pSiNPs from single-crystal silicon wafers with high reproducibility in a single 24 h process. The performance of the produced pSiNPs is validated in a drug delivery application in which loading and release of the anthracycline drug doxorubicin are compared with pSiNPs prepared in a conventional cleaning bath ultrasonicator.

KEYWORDS: electrochemical anodization, drug delivery system, nanoparticle preparation, ultrasonication, gram-scale fabrication

1. INTRODUCTION

Biological applications of porous silicon nanoparticles (pSiNPs) include drug delivery systems, 1,2 bioimaging, 3 and biosensing.⁴ For these applications, various surface chemistries,5 drug- or imaging agent-encapsulation strategies,6 and particle size control methods have been explored to enable or extend the utility of pSiNPs.7 The process used to prepare pSiNPs, involving electrochemical anodization of high-purity single-crystal silicon wafers, provides very precise control of nanostructure in the material.8 Despite the improved in vitro and in vivo performance of the material, one of the major challenges of pSiNPs is their high cost relative to other nanoparticle systems, such as sol-gel-derived mesoporous silica nanoparticles, polymer nanoparticles, or liposomes. While there are now commercial sources of pSiNPs (for example, TruTag Technologies, https://trutags.com/), 10 largescale, reproducible preparation methods for high-purity pSiNPs are lacking.¹¹ Thus, it is necessary to develop a new method for manufacturing large-scale and reproducible pSiNPs to reduce the manufacturing cost of pSiNPs and increase their utilization. Generally, pSiNPs are prepared from single-crystal Si wafers in two steps: (i) an electrochemical etching and liftoff process that generates a free-standing film of porous Si

(pSi) with the desired pore diameters and pore wall thickness (Figure 1a) and (ii) a fracturing step that breaks the pSi film into nanoparticles of the desired size (Figure 1b). There have been many methods deployed in the fracturing step, such as physical grinding or ball-milling, 13-17 lithography, 18,19 ultrasonication, 20,21 and microfluidization. These methods all aim to increase the yield and reproducibility for the preparation of large quantities of pSiNPs while maintaining control over critical properties such as nanoparticle size and size distribution, pore size, surface chemistry, and molecular loading/release characteristics according to their intended use. Among the methods, the ultrasonic method is most common because it can be used without expensive equipment—typically, a commercial ultrasonic cleaning bath is used. However, an ultrasonic cleaner-based approach is particularly challenging for large-scale preparation of pSiNPs

Received: February 13, 2024 Revised: April 1, 2024 Accepted: April 6, 2024



ACS Applied Nano Materials

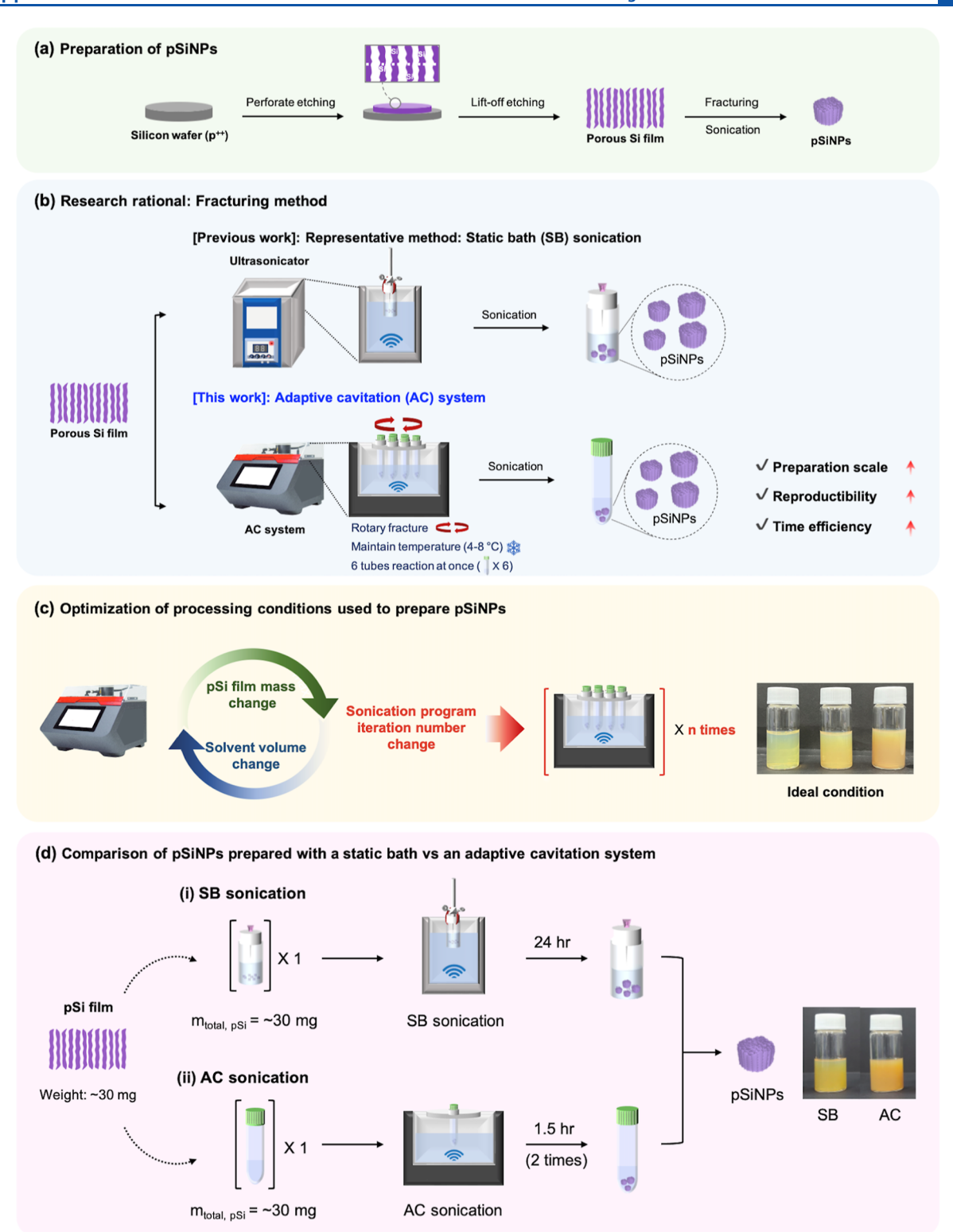


Figure 1. (a) Schematic illustration of the electrochemical etching process and fabricating pSiNPs. (b) Schematic illustration of the pSiNP fracturing process using SB sonication and an AC system and the advantages of pSiNP fabrication through this work. (c) Schematic diagram of optimization experiments to maximize the yield of pSiNPs using an AC system. Yield variation of pSiNPs with changes in the pSi film mass, solvent volume, and sonication program iteration number. (d) Schematic diagram of the pSiNP fabrication process following the SB sonication protocol and the optimized AC system protocol, along with the corresponding result images.

because the baths tend to heat up during operation, they do not provide uniform ultrasound fields, and they require long $(16-24~\mathrm{h})$ reaction times for the pSiNPs to reach the desired sizes. ^{24,25} The main sources of losses in the procedure result

from these limitations: heating of the bath can cause oxidation and dissolution of the silicon material, which is exacerbated at longer sonication times, and the nonuniform ultrasound fields lead to incomplete fracture of the pSi films, resulting in larger fragments that do not fracture into nanometer sizes. Both of these factors can substantially reduce the yield of nanoparticles. ²²

Commercial sonicators that have been developed to process biological samples (for DNA and chromatin shearing, cell lysis, tissue disruption, and DNA/RNA extraction) have solved similar issues of sample degradation and uniformity and provide a potential solution for scale-up of pSiNP production (Figure 1b). The commercial Bioruptor sonicator from Diagenode was used in the present study. Marketed as an "adaptive cavitation (AC)" system, this ultrasonic bath uses a sample rotation stage, a refrigerator (4 °C), and userprogrammable on-off cycles to better control the uniformity of the sheared products. It also allows modest user control of the ultrasound frequency and power, providing an additional means of process optimization. In this work, we systematically optimized these and other parameters with the aim of providing a gram-scale preparation of size-controlled pSiNPs (Figure 1c). Then, we benchmarked the properties of the resulting pSiNPs in a drug delivery type of application against the well-established sonication method based on a static bath (SB) (Figure 1d). In particular, since we obtained gram-scale and reproducible pSiNPs with this method, we present a new way to address the scale-up and reproducibility limitations of pSiNP preparation that were difficult to overcome with existing methods. We expect to contribute to the economic improvement of pSiNP preparation and utilization.

2. RESULTS AND DISCUSSION

2.1. Sonication by Adaptive Cavitation. The relevant parameters for the AC sonication and SB sonication methods used in this study are given in Table 1. The key differences are that AC includes a rotating sample stage to spread the ultrasound energy more evenly through the samples, and it also alternates between on and off states for controllable periods of time, which allows heat generated in the samples by the

Table 1. Comparison of SB Sonication and AC Sonication

properties	SB ^a sonication	AC ^a sonication
power (frequency)	48 W (~35 kHz)	150 W (~40 kHz)
sonication type	continuous	50% duty cycle (on/off)
number of vessels used in the reactor at one time	1	6
temperature control and range	none (25–65° C)	active (4–8°C) (cooler/circulator)
processing time per single porous Si film sample	>24 h	2-6 h
solvent used (volume)	EtOH (~6 mL)	EtOH (≤2 mL)
reactor material (volume)	glass vial (~20 mL)	polypropylene tube (15 mL)
volume of water in the sonication bath	~1900 mL	700 mL
nanoparticle yield (from 30 mg of pSi film)	$34.5 \pm 1.64\%$	$50.3 \pm 0.82 -$ $58.6 \pm 1.33\%$

""Static bath" refers to a conventional ultrasonic cleaner equipped with a water tank without active cooling or stirring (VWR Symphony ultrasonic cleaner, model VWRA142-0307). "Adaptive cavitation" refers to an ultrasonic bath equipped with a sample rotation stage and active cooling, with ultrasound power delivered in a series of on—off cycles (Diagenode Bioruptor Pico sonication device, model B01080010).

ultrasound energy to dissipate into a thermostated water bath. Unlike a static ultrasound cleaner, the sonication frequency and power were also adjustable. For this study, it was found that ultrasound of a frequency of 40 kHz was more effective at fragmenting the pSi films into nanoparticles than the 35 kHz frequency more commonly used in ultrasonic cleaners. It includes all the effects, such as the frequency-dependent properties of the sonication wave (the straightness of the sonication wave, the formation, and behavior of cavitation bubbles)²⁶ the difference in power, the rotating sample stage, and the maintained temperature (4-8 °C). The higher the frequency of the ultrasonication, the stronger the straightness of the sonication wave and the faster the decomposition rate of the cavitation bubbles formed in the tube. It reduces the loss of sonication energy due to the medium and bubbles and increases the total energy transferred to the pSi film. Therefore, since the fragmenting efficiency of the pSi film increases, pSiNPs are produced more efficiently when the frequency is high. In addition, in the case of AC sonication, the power is 3.1 times higher than that of SB sonication, and considering the difference in acoustic pressure due to the power difference, the fragmenting efficiency of the pSi film is even higher. The AC unit allowed independent control of the duty cycle (the ON and OFF times in a given cycle), the number of cycles in an iteration, and the total number of iterations. The thermostat in the unit was aided by a circulator in order to maintain a constant temperature inside the sonicator bath. The rotating sample stage in the AC sonicator used in this study held six sample vials, allowing for higher throughput than that in the static immersion bath. These features all provide convenient avenues for process optimization.

2.2. Optimization of Processing Conditions. The processing of pSi films into pSiNPs using AC sonication followed two main steps: the as-prepared pSi films were fractured in the AC sonicator following a set protocol (see below), and then they were washed by centrifugation with no additional filtration steps. The centrifugation washing involved two steps: a low-speed step that removed the larger (>1 μ m) fragments and a high-speed step that isolated the desired nanoparticles from the smaller (<50 nm) particles. While the perforated etch used in the preparation of the pSi films generates a nanostructure that tends to break into a specific size of nanoparticles, the process also generates particles outside of the specified size range.²¹ The larger fragments are thought to result from incomplete fracture, while the smaller particles are attributed to overfracturing of the nanoparticles and reprecipitation of molecular silicate species that dissolve during ultrasonic processing. The purpose of the low-speed centrifugation step was to pelletize the larger particles and leave the desired nanoparticles (along with undesired smaller nanoparticles) in the supernatant, whereas the purpose of the high-speed step was to pelletize the desired pSiNPs while leaving the smaller fragments suspended in the supernatant. These larger and smaller fragments contributed to lowered yields, which the process optimization protocol followed in the present study was designed to minimize. The resulting pSiNPs (named AC-pSiNPs) were then quantified and characterized.

The AC protocol (instrumental default) involved a cycle with a fixed on-time of 30 s, followed by an off-time of 30 s. The "on-time" in a given cycle corresponded to the application of 150 W of 40 kHz ultrasound to the reaction chamber. A single on—off cycle was then repeated 30 times, representing one iteration of 30 min duration. One 30 min iteration was

ACS Applied Nano Materials www.acsanm.org

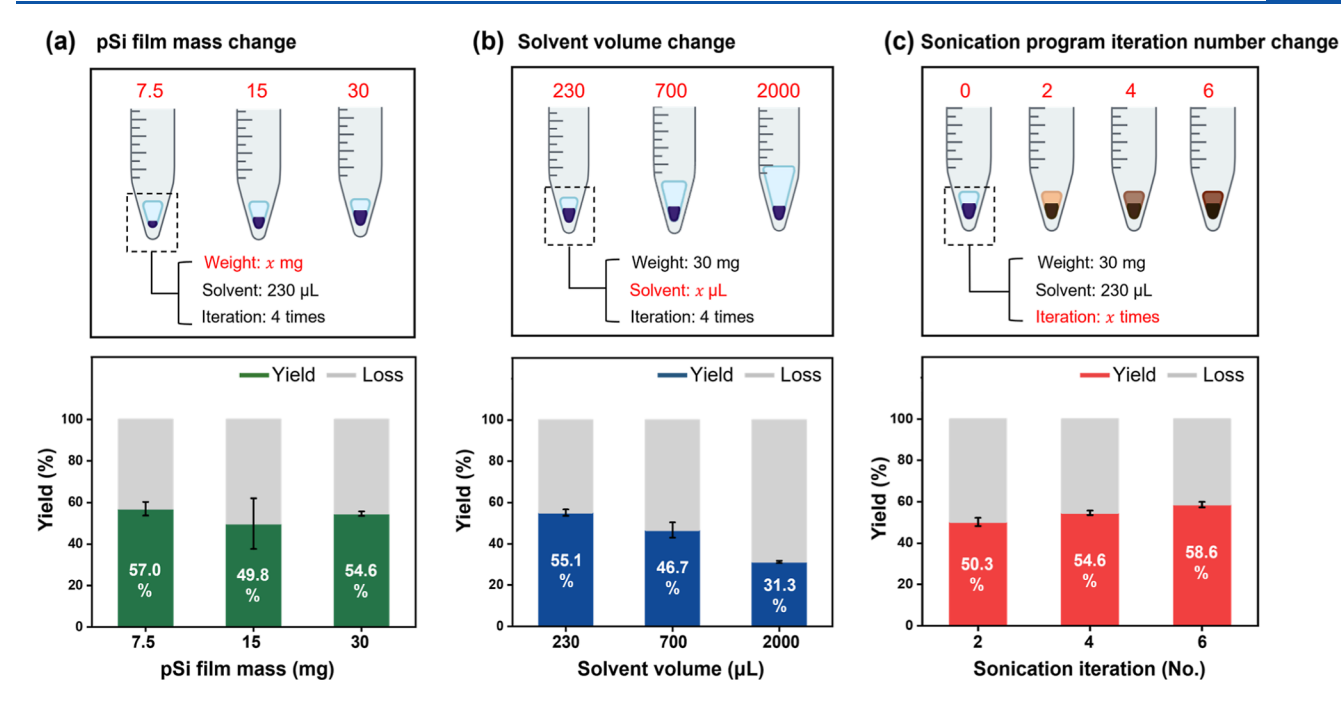


Figure 2. Optimization experiments to maximize the yield of pSiNPs using AC sonication. Yield variation of pSiNPs with changes in the (a) pSi film mass, (b) solvent volume, and (c) sonication program iteration number. Error bars represent the standard deviation from n = 3 measurements.

then optionally repeated for a maximum of 6 iterations. If an additional iteration was used before the application of ultrasound, the sample was allowed to rest for 30 min; it remained in the thermostated reaction chamber and continued to rotate to equilibrate the temperature and allow the ultrasound transducers to recover.

In general, one electrochemical etching and lift-off process on a Si wafer can generate approximately ~30 mg of pSi film. Then, the pSi film fractures in the EtOH solvent by AC sonication. The optimal processing conditions were determined by adjusting the mass of the pSi film and the solvent volume used in a given sonication run (Table 1). The size of the tubes for these studies was fixed at 15 mL (solvent maximum volume in a tube: 2 mL). The results of varying the mass of the pSi film used in the reaction tubes while keeping other parameters fixed are presented in Figures 2a and S1. The resulting AC-pSiNPs were characterized by dynamic light scattering (DLS) analysis and attenuated total reflectance Fourier transform infrared (ATR-FTIR) spectroscopy, which provided readouts on the average nanoparticle size, width of the size distribution, surface charge, and surface chemistry.

In order to evaluate the effect of the mass of the pSi film used in the process, 7.5, 15, and 30 mg of pSi were each added to reaction vials, and the solvent volume (EtOH, 230 μL) in each vial and the sonication iteration number (4 times) were maintained constant. The yield of pSiNPs resulting from each experiment was determined by freeze-drying mass measurements. The percent yield of pSiNPs for the samples containing 7.5, 15, and 30 mg of pSi film were 57.0 \pm 3.3, 49.8 \pm 12.2, and $54.6 \pm 1.1\%$, respectively (Figure 2a). The difference in percent yield was not statistically significant, suggesting that the process was sufficient to generate pSiNPs from a pSi film over the entire experimental mass range studied. Therefore, the subsequent optimization experiments used 30 mg of pSi film in order to maximize the quantity of pSiNPs produced in a run. The pSiNPs obtained in the three cases showed a consistent mean hydrodynamic diameter of approximately 175 nm and a narrow distribution of particle sizes (polydispersity index, PDI: 0.15–0.20), as measured by DLS analysis. The DLS measurements yielded zeta-potential values of approximately –6.4 mV for all the preparations. The negative surface charge is consistent with ATR-FTIR spectra (Figure S2) of the nanoparticles, which revealed the presence of Si–O–Si and Si–OH species that are indicative of surface oxidation. Silicon oxides generally exhibit a negative surface charge in water. ^{27,28}

Article

Next, the effect of the solvent volume on the efficiency of nanoparticle generation was studied. A fixed mass of the pSi film (30 mg) was dispersed in sample tubes containing 230, 700, and 2000 μ L of EtOH, and they were subjected to identical sonication conditions (iteration number = 4). The yield of pSiNPs was found to show a pronounced dependence on volume; for solvent volumes of 230, 700, and 2000 μ L, the yield values were 55.1 \pm 1.6, 46.7 \pm 3.7, and 31.3 \pm 0.6%, respectively (Figure 2b). The yields decreased with an increasing solvent volume. It is due to the solvent and cavitation bubble effect. The smaller the volume of the solvent, the less energy loss by the solvent, and the smaller the cavitation bubble generated in the tube, the more significant the total amount of energy transferred to the pSi film, which increases the fragmenting efficiency.

The quality of the nanoparticles produced was also dependent on the solvent volume. The hydrodynamic diameter of pSiNPs increased with increasing solvent volume (Figure S3). The PDI did not differ substantially for the different preparations, although it was the smallest for the intermediate volume (700 μ L).

Lastly, the effect of the iteration number, i.e., the number of times that the reaction vials were subjected to ultrasound cycles, was tested. Based on the improved yield, we chose 230 μ L for the solvent volume and 30 mg for the mass of the pSi film used in one reaction vial for these studies (Figure 2b). The sonication iteration number was tested 2, 4, and 6 times, and the yield of pSiNPs was compared. For iteration numbers 2, 4, and 6, the yield values were 50.3 \pm 2.0, 54.6 \pm 1.1, and 58.6 \pm

ACS Applied Nano Materials

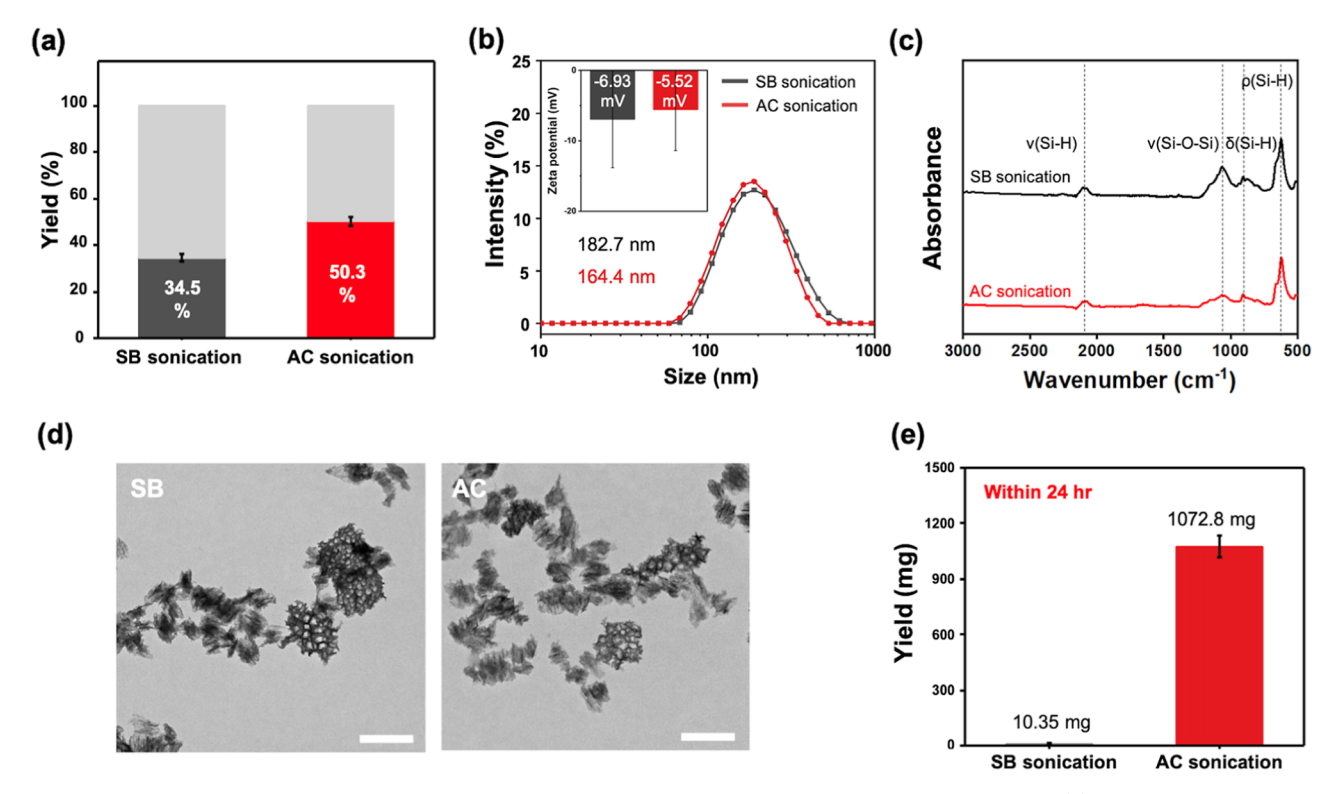


Figure 3. Comparison of the characteristics of pSiNPs prepared by SB sonication and by the AC system method. (a) Yield of pSiNPs by the SB sonication protocol and the optimized AC system protocol. (b) Average hydrodynamic diameter and zeta-potential value of pSiNPs fabricated by the SB sonication protocol and the optimized AC system analyzed by DLS. PDI: SB sonication = 0.172 ± 0.0214 and AC system = 0.151 ± 0.0275 . (c) ATR-FTIR spectra of pSiNPs fabricated by a SB and an AC system. Symbols: ν = stretching, δ = bending, and σ = rocking. (d) TEM images of pSiNPs fabricated by SB and dynamic bath systems. Scale bar: 400 nm. (e) Operating for 24 h and the resulting yield under those conditions using SB and AC sonication.

1.3%, respectively (Figure 2c). Thus, the yields tended to increase slightly with the increasing iteration number (corresponding to increased sonication time).

These results led to an optimized protocol as follows:

- Reaction tubes: 6 × 15 mL
- Volume of EtOH per tube: 230 μ L
- Mass of pSi flakes added per tube: 30 mg
- On-off cycle: 30 s on, 30 s off
- Number of on—off cycles: 30
- Number of iterations: 6
- Rest period between iterations: 30 min
- Ultrasound power: 150 W
- Ultrasound frequency: 40 kHz
- Total treatment time: 5.5 h
- Mass of pSiNPs resulting: 105 mg

It was confirmed that the yield of the optimized conditions $(55 \pm 3\%)$ was comparable to the highest yield (57%) reported for the microfluidization method. These results confirmed that AC sonication for the preparation of pSiNPs is faster with higher yields compared to conventional SB sonication. In addition, pSiNPs obtained from the optimized protocol showed a homogeneous mean hydrodynamic diameter of approximately 170 nm with a high size uniformity (PDI: 0.15) and a negative zeta potential of approximately -6.0 mV (Figure S4).

2.3. Comparison of pSiNPs Prepared with a SB vs an AC System. To more directly compare the properties of pSiNPs, the pSiNPs were prepared from the same pSi film feedstock but then fractured either using SB or AC sonication. The resulting nanoparticles are here referred to as SB-pSiNPs

or AC-pSiNPs, respectively. The SB-pSiNPs were prepared using SB sonication (30 mg of pSi film mass, 6 mL of EtOH, and 24 h sonication), and the AC-pSiNPs were prepared using AC sonication [30 mg of pSi film mass, 230 μ L of EtOH, and two iterations of sonication (1.5 h processing time)]. The characterization of both SB- and AC-pSiNPs in terms of yield, DLS and ATR-FTIR analysis, and transmission electron microscopy (TEM) measurement, is given in Figure 3a–d.

The yields of as-prepared SB-pSiNPs and AC-pSiNPs were 37.3 and 50.3%, respectively (Figure 3a). Both batches of particles showed a similar homogeneous mean hydrodynamic diameter of 182.7 \pm 94.8 nm (SB-pSiNPs) and 164.4 \pm 78.0 nm (AC-pSiNPs) with a comparable size uniformity (PDI: 0.17 for SB-pSiNPs and 0.15 for AC-pSiNPs). The zeta potential was -6.9 and -5.5 mV for SB-pSiNPs and ACpSiNPs, respectively (Figure 3b). The ATR-FTIR spectra (Figure 3c) indicated that the pSiNPs made in the SB (SBpSiNPs) had a somewhat higher degree of oxidation than that of the AC-pSiNPs, which is consistent with the longer reaction time and higher temperature of the SB sonication process. The infrared spectrum of both types of pSiNPs displayed two characteristic bands associated with surface hydrides: $\nu(Si-H)$ stretching at 2050-2100 cm⁻¹, δ (Si-H) bending at 873 cm^{-1,30} and ρ (Si–H) rocking at 621 cm⁻¹ and surface oxides: $\nu(\text{Si-O-Si})$ stretching at 1100–1000 cm^{-1,31,32} In addition, TEM images of SB-pSiNPs and AC-pSiNPs showed that both nanoparticle types had similar sizes and porous nanostructures, with average pore sizes of 20.58 ± 4.47 nm for SB-pSiNPs and 19.72 ± 3.82 nm for AC-pSiNPs (Figures 3d and S5). Total pore volumes and average pore sizes were calculated from

Table 2. Texture Properties of pSiNPs Made by SB Sonication and AC Sonication

properties	size (nm)	zeta potential (mV)	pore size (TEM) (nm)	pore size (BJH) (nm)	pore volume (cm³/g)	BET surface area (m^2/g)
SB-pSiNPs	182.7	-6.93	20.58 ± 4.47	20.06	3.81	1079
AC-pSiNPs	164.4	-5.52	19.72 ± 3.82	19.49	3.51	1180
(a)	SB-pSiNPs AC-pSiNPs	Doxorub Dox	DOX@SB-pSiNPs DOX@AC-pSiNPs	(b) 25 — DOX@SB-pSiNPs — DOX@AC-pSiNPs 257.0 nm 257.0 nm Size (nm)	1000	41.7 44.0 mV
Absorbance (H-O)A	SiNPs @SB-pSiNPs @AC-pSiNPs	v(Si-O) DOX@SB-pSiNP	s DOX@AC-pSiNPs	Coading efficiency (%) 100 100 100 100 100 100 100 100 100 10	(g) (%) 80- juid essel 20- 32.7%	DOX@SB-pSiNPs DOX@AC-pSiNPs 10 15 20 25
	Wavenumber (cm ⁻¹)	1000		DOX@SB-pSiNPs DOX	(@AC-pSiNPs	Time (h)

Figure 4. Comparison of the characteristics of DOX-loaded pSiNPs prepared by SB and AC sonication methods. (a) Illustration of the loading of DOX into the pSiNPs. The drug loading protocol was identical for both nanoparticle types. DOX@SB-pSiNPs represent DOX-loaded pSiNPs prepared via the SB sonication method and DOX@AC-pSiNPs represent DOX-loaded pSiNPs prepared via the AC sonication method. (b) Intensity histograms from DLS measurements showing the average hydrodynamic diameter of the two drug-loaded nanoparticle types (PDI: DOX@SB-pSiNPs = 0.357 \pm 0.0431 and DOX@AC-pSiNPs = 0.241 \pm 0.0398). (c) Zeta-potential values determined from DLS measurement of empty and DOX-loaded pSiNPs prepared by SB or AC sonication. (d) ATR-FTIR spectra of DOX-loaded pSiNPs fabricated by AC and SB sonication. Symbols: ν = stretching and δ = bending. (e) TEM images of DOX-loaded pSiNPs synthesized by SB and AC sonication. (g) Comparison of the cumulative amount of DOX released from the pSiNPs synthesized by SB and AC sonication of time, incubated in PBS (1×, pH 7.4) at 37 °C.

nitrogen adsorption—desorption isotherms (Figure S6) using the Brunauer—Emmett—Teller (BET) method.³³ The total pore volume and average pore size for SB-pSiNPs were 3.81 cm³/g and 20.06 nm, respectively, and for AC-pSiNPs, they were 3.51 cm³/g and 19.49 nm (Table 2). These results indicated that AC-pSiNPs had the same material characteristics as SB-pSiNPs. The amount of pSiNPs that could be prepared with the two processing systems in a given 24 h period was quite different (Figure 3e). The SB system generated 11.17 mg, while the AC system produced 1072.8 mg in the same 24 h period. The difference is due to the combination of the higher yield of AC sonication, the reduced per-vial processing time, and the ability of the AC system to accommodate six vials in its rotating carousel. This is the first report that confirms the possibility of gram-scale preparation of pSiNPs within 1 day.

2.4. Benchmarking of pSiNP Performance with a Model Drug (Doxorubicin). The performance of the optimized pSiNP preparation was next evaluated in a simple drug loading experiment. pSiNPs formed by SB sonication have been shown to load the anthracycline drug doxorubicin (DOX) and the related drug daunorubicin with a good efficiency (Figure 4a).^{34–40} We loaded DOX into samples of both SB-pSiNPs and AC-pSiNPs that were prepared as described in the previous section and characterized as shown in Figure 3. Both nanoparticle types were loaded with DOX following identical loading protocols, and the resulting samples are here designated DOX@SB-pSiNPs for doxorubicin-loaded pSiNPs prepared via the SB sonication method and DOX@

AC-pSiNPs for doxorubicin-loaded pSiNPs prepared via the AC sonication method. The loading chemistry for DOX, referred to as oxidative loading, involves treating the nanoparticles in an aqueous solution containing the drug. The driving force for this reaction is the oxidation of Si to SiO₂, referred to as "oxidative trapping". The starting pSiNPs contain a thin shell of oxide and hydroxide over an elemental silicon core. During the 24 h loading period, the elemental silicon in the core oxidizes, and the resulting oxide dissolves and then reprecipitates within the pores, causing a restructuring of the pores that traps the payload. 41 After DOX loading into the pSiNPs, the resulting DOX@SB-pSiNPs and DOX@ AC-pSiNPs both showed a slight increase in size, and the size distribution remained uniform: DOX@SB-pSiNPs: 257.0 ± 77.3 nm (PDI: 0.35); DOX@AC-pSiNPs: 276.2 ± 90.2 nm (PDI: 0.24), Figure 4b. The zeta-potential values of SBpSiNPs, DOX@SB-pSiNPs, AC-pSiNPs, and DOX@ACpSiNPs were -41.1 ± 25.0 , -40.4 ± 22.0 , -41.7 ± 24.4 , and -40.4 ± 19.2 mV, respectively (Figure 4c). The ATR-FTIR spectra of samples of DOX-loaded and -empty pSiNPs were also acquired to observe the surface functionality (Figure 4d). The infrared spectrum of pSiNPs displayed four characteristic bands associated with the silanol (Si-OHs) functionality: $\nu(O-H)$ peak at 3550-3200 cm⁻¹, ⁴² $\nu(Si-H)$ peak at 2104 nm⁻¹, δ (O–H) peak at 1632 cm⁻¹, and ν (Si–O) peak at 1064 nm⁻¹.2,43,44 On the other hand, ν (C=O) peak at 1719 cm⁻¹ and ν (C=C) peak at 1615 and 1412 cm⁻¹ of DOX were additionally observed in DOX-loaded pSiNPs. 45 TEM

images indicated that the homogeneous size and the porous nanostructure of both types of drug-loaded pSiNPs, DOX@ SB-pSiNPs and DOX@AC-pSiNPs, were preserved with no significant pore wall collapse during the drug loading process (Figure 4e). In addition, both SB- and AC-pSiNPs loaded with DOX showed a high loading efficiency of the DOX drug (DOX@SB-pSiNP: $30.8 \pm 5.1\%$ and DOX@AC-pSiNP: 32.7 \pm 1.5% by mass) (Figure 4f). The loading of DOX within the pores of pSiNPs was verified by incubation of both SB- and AC-pSiNPs in DI H₂O for 24 h at 25 °C and assays of the supernatant after the centrifugal removal of the particles. To evaluate the temporal drug release profile from both SB- and AC-pSiNPs, we dispersed both SB- and AC-pSiNPs loaded with DOX in phosphate-buffered saline solutions (1× PBS, pH 7.4) for 24 h and assayed the supernatants for free DOX at regular time intervals (Figures 4g and S6). The majority of the drug load (50%) was released within 4 h, and the remaining drug was released within 24 h. These results confirmed that AC-pSiNPs and SB-pSiNPs have similar drug loading/release properties.

3. CONCLUSIONS

A method for preparing gram-scale quantities of pSiNPs with high reproducibility is demonstrated by using AC sonication. The AC sonication was able to induce stable, high yields through rotary fracture, maintaining a temperature of 4-8 °C, and using 6 tubes at a time. Based on these properties, the AC sonication process was optimized by adjusting the pSi film mass, solvent volume, and sonication iteration number. Moreover, upon comparison of pSiNPs manufactured using bath-based sonication, AC-pSiNPs showed similar material properties, such as size and size distribution, surface chemistry, and drug loading/release characteristics. By combining optimized preparation conditions, AC sonication demonstrated higher yields (by 1.4-fold), reduced total processing time (by 12-fold), and the ability of the commercial reactor to hold six reaction vials in one carousel improved throughput by 6fold. This resulted in a benchtop process for the generation of gram-scale quantities of pSiNPs with high reproducibility in a 24 h period (increasing production by ~100-fold over SB sonication).

4. EXPERIMENTAL SECTION

- **4.1. General Information.** General information on reagents, instruments, and analytical methods used in this study is available in the Supporting Information.
- 4.2. Preparation of pSi Films. pSi films were prepared by galvanostatic anodization of p-type single-crystal silicon wafers (heavily boron-doped, resistivity $\sim 1~\text{m}\Omega$ cm) in an electrolyte consisting of 3:1 (v/v) 48% aqueous HF: absolute ethanol (EtOH) [caution: HF is highly toxic, and proper care should be used to avoid contact with the skin or lungs]. Before the preparation of the pSi layers, the silicon wafer was first cleaned by anodization in the HFcontaining electrolyte to generate a thin porous layer, commonly referred to as a "sacrificial layer", and the resulting porous layer was then dissolved by treatment with aqueous potassium hydroxide (KOH, 2 M). The silicon wafer was then anodized using a "perforated etch",21 which involved the application of an etching waveform that consisted of a lower current density of 440 mA cm⁻² applied for 1.8 s, followed by a higher current density pulse of 3210 mA cm⁻² applied for 0.4 s. This waveform was repeated for 300 cycles, generating a pSi film with high porosity "perforations" repeating approximately every 200 nm through the porous layer. The pSi film was then removed from the silicon substrate by application of a current density of 38 mA cm⁻² for 300 s in a solution containing an electrolyte of 1:12 (v/v) of

48% aqueous HF: EtOH. The free-standing fragments of the pSi film were then rinsed thoroughly with EtOH and placed in EtOH in a sealed glass vial.

- **4.3. Preparation of pSiNPs Using a Conventional Immersion Bath Ultrasonicator.** The control pSiNPs were generated from the free-standing pSi film by placing a predetermined mass of the film in a 20 mL glass vial containing 6 mL of EtOH. The vial was sealed and then suspended in the 1.9 L water reservoir of a Symphony ultrasonic cleaner (VWR, model VWRA142-0307) operating at 35 kHz and subjected to continuous ultrasound for 24 h. While the bath volume was maintained at \sim 1.9 L by the use of a siphon from an external water reservoir, no attempt was made to control the bath temperature. The larger, unfractured particles remaining after the process were separated by centrifugation at 845 rcf for 15 min, and the pellet was discarded. The supernatant was then centrifuged at 21,130 rcf for 15 min and washed 3 times by resuspension/centrifugation at 21,130 rcf with EtOH. For the determination of yield, samples were freeze-dried and weighed on an analytical balance.
- **4.4.** Preparation of pSiNPs Using AC Ultrasonication. The pSi film was placed in a 15 mL "Bioruptor Pico Tube" obtained from Diagenode containing EtOH (maximum volume: 2 mL) and fractured by AC ultrasonication. One iteration of the AC ultrasonication had the following settings: sonication ON: 30 s; sonication OFF: 30 s; number of cycles: 30 cycles; type of tubes: 15 mL; and total running time: 30 min. After one iteration, the device was allowed to rest for 30 min prior to the initiation of the next iteration (if desired). Then, large-size unfractured particles were separated by centrifugation at 3000 rpm for 15 min. The precipitated pSiNPs were discarded, and the supernatant was centrifuged at 21,130 rcf for 15 min and washed 3 times with EtOH. For the determination of yield, samples were freezedried and weighed on an analytical balance.
- **4.5. Drug Loading and Release Assay.** pSiNPs (\sim 1 mg) were agitated with 100 μ L of DOX stock solution (10 mg/mL in DI H₂O) in 900 μ L of DI H₂O for 24 h. The resulting nanoparticles were washed with DI H₂O using the centrifuge (21,130 rcf, 15 min, and 3 times). The emission spectra of the supernatants at each washing step were measured ($\lambda_{\rm exc.max}$ = 488 nm and $\lambda_{\rm emi.max}$ = 595 nm) to determine the quantity of unloaded drug. The mass loading of DOX was determined using the following equation

loading efficiency (%) =
$$\frac{W_{\text{total DOX}} - W_{\text{unloaded DOX}}}{W_{\text{total DOX}}} \times 100$$
 (1)

The value of the mass of DOX loaded was determined as the difference between the mass of DOX in the loading solution prior to the addition of the nanoparticles and the mass of DOX remaining in the supernatant after the DOX-loaded nanoparticles were removed by centrifugation. This calculation assumes no loss of nanoparticles due to dissolution. The solution concentrations of DOX were calculated from standard fluorescence curves by using OriginPro software (Northampton, MA, USA).

The release profile of nanoparticles was analyzed by measuring the fluorescence of the drug remnants in phosphate-buffered saline (PBS, pH 7.4) at each time interval for 24 h at 37 $^{\circ}$ C.

ASSOCIATED CONTENT

5 Supporting Information

The Supporting Information is available free of charge at https://pubs.acs.org/doi/10.1021/acsanm.4c00908.

General information, experimental details, and supporting figures: porous silicon nanoparticle image during the optimization process; characterization of pSiNPs fabricated by AC sonication according to the pSi film mass change, solvent volume, and sonication iteration number; TEM images and statistical analysis of the average pore diameter of pSiNPs fabricated by AC and SB sonication; and DOX loading/release profile (PDF)

AUTHOR INFORMATION

Corresponding Authors

Dokyoung Kim – Department of Precision Medicine, Graduate School, Kyung Hee University, Seoul 02447, Republic of Korea; Department of Biomedical Science, Graduate School, College of Medicine, Department of Anatomy and Neurobiology, College of Medicine, Center for Converging Humanities, and KHU-KIST Department of Converging Science and Technology, Kyung Hee University, Seoul 02447, Republic of Korea; UC San Diego Materials Research Science and Engineering Center, La Jolla, California 92093, United States; Medical Research Center for Bioreaction to Reactive Oxygen Species and Biomedical Science Institute, Core Research Institute (CRI), Kyung Hee University, Seoul 02447, Republic of Korea; Center for Brain Technology, Brain Science Institute, Korea Institute of Science and Technology (KIST), Seoul 02792, Republic of Korea; orcid.org/0000-0002-7756-3560; Email: dkim@ khu.ac.kr

Hwajun Jeong — College of Medicine, Kyung Hee University, Seoul 02447, Republic of Korea; Medical Research Center for Bioreaction to Reactive Oxygen Species and Biomedical Science Institute, Core Research Institute (CRI), Kyung Hee University, Seoul 02447, Republic of Korea; Email: hjjeong0923@gmail.com

Jaehoon Kim – College of Medicine, Kyung Hee University, Seoul 02447, Republic of Korea; Email: jk.chembiologist@gmail.com

Michael J. Sailor — Department of Chemistry and Biochemistry, University of California San Diego (UCSD), La Jolla, California 92093, United States; Department of Nanoengineering, University of California, La Jolla, California 92093, United States; UC San Diego Materials Research Science and Engineering Center, La Jolla, California 92093, United States; orcid.org/0000-0002-4809-9826; Email: msailor@ucsd.edu

Authors

Jaehui Lee – Department of Precision Medicine, Graduate School, Kyung Hee University, Seoul 02447, Republic of Korea

Hye Ji Um – Department of Biomedical Science, Graduate School, Kyung Hee University, Seoul 02447, Republic of Korea

Complete contact information is available at: https://pubs.acs.org/10.1021/acsanm.4c00908

Notes

The authors declare the following competing financial interest(s): The authors are listed as inventors on a pending patent application related to the technology described in this work. MJS is a scientific founder (SF), member of the Board of Directors (BOD), Advisory Board (AB), Scientific Advisory Board (SAB), acts as a paid consultant (PC) or has an equity interest (EI) in the following: Aivocode, Inc (AB, EI); Bejing ITEC Tech-nologies (SAB, PC); Illumina (EI), Impilo Therapeutics (SAB, EI), Lisata Therapeutics (EI); Matrix Technologies (EI); Precis Therapeutics (SF, BOD, EI), Quanterix (EI), Spinnaker Biosciences, Inc. (SF, BOD, EI); TruTag Tech-nologies (SAB, EI); and Well-Healthcare Technologies (SAB, PC). Although one or more of the grants that supported this research have been identified for conflict-of-interest management based on the overall scope of the

project and its potential benefit to the companies listed, the research findings included in this publication may not necessarily relate to their interests. The terms of these arrangements have been reviewed and approved by the University of California, San Diego in accordance with its conflict-of-interest policies.

ACKNOWLEDGMENTS

This work was supported by a grant from the Bio & Medical Technology Development Program of the National Research Foundation (NRF) of Korea, funded by the Ministry of Science & ICT (2021-M3A9I5030523; D.K.). This research was also supported by the Basic Science Research Program through the NRF of Korea, funded by the Ministry of Education (2018-R1A6A1A03025124; D.K.) and the NRF grant funded by the Korean government (MSIT) (2022-R1F1A1069954; D.K.). This research was partially supported by NSF through the UC San Diego Materials Research Science and Engineering Center (UCSD MRSEC), grant DMR-2011924. The authors acknowledge the use of facilities and instrumentation supported by NSF through the UC San Diego Materials Research Science and Engineering Center (UCSD MRSEC) DMR-2011924.

REFERENCES

- (1) Fontana, F.; Shahbazi, M. A.; Liu, D.; Zhang, H.; Mäkilä, E.; Salonen, J.; Hirvonen, J. T.; Santos, H. A. Multistaged nanovaccines based on porous silicon@ acetalated dextran@ cancer cell membrane for cancer immunotherapy. *Adv. Mater.* **2017**, 29 (7), 1603239.
- (2) Kim, J.; Um, H.; Kim, N. H.; Kim, D. Potential Alzheimer's disease therapeutic nano-platform: Discovery of amyloid-beta plaque disaggregating agent and brain-targeted delivery system using porous silicon nanoparticles. *Bioact. Mater.* **2023**, *24*, 497–506.
- (3) Wu, S.; Zhong, Y.; Zhou, Y.; Song, B.; Chu, B.; Ji, X.; Wu, Y.; Su, Y.; He, Y. Biomimetic preparation and dual-color bioimaging of fluorescent silicon nanoparticles. *J. Am. Chem. Soc.* **2015**, *137* (46), 14726–14732.
- (4) Bu, Y.; Zhu, G.; Li, S.; Qi, R.; Bhave, G.; Zhang, D.; Han, R.; Sun, D.; Liu, X.; Hu, Z.; et al. Silver-nanoparticle-embedded porous silicon disks enabled SERS signal amplification for selective glutathione detection. ACS Appl. Nano Mater. 2017, 1 (1), 410–417.
- (5) Jung, Y.; Huh, Y.; Kim, D. Recent advances in surface engineering of porous silicon nanomaterials for biomedical applications. *Microporous Mesoporous Mater.* **2021**, 310, 110673.
- (6) Zhang, H.; Liu, D.; Shahbazi, M. A.; Mäkilä, E.; Herranz-Blanco, B.; Salonen, J.; Hirvonen, J.; Santos, H. A. Fabrication of a multifunctional nano-in-micro drug delivery platform by microfluidic templated encapsulation of porous silicon in polymer matrix. *Adv. Mater.* **2014**, 26 (26), 4497–4503.
- (7) Secret, E.; Leonard, C.; Kelly, S. J.; Uhl, A.; Cozzan, C.; Andrew, J. S. Size control of porous silicon-based nanoparticles via pore-wall thinning. *Langmuir* **2016**, 32 (4), 1166–1170.
- (8) Chiappini, C.; Tasciotti, E.; Fakhoury, J. R.; Fine, D.; Pullan, L.; Wang, Y. C.; Fu, L.; Liu, X.; Ferrari, M. Tailored porous silicon microparticles: fabrication and properties. *ChemPhysChem* **2010**, *11* (5), 1029–1035.
- (9) Yan, Z.; Jiang, J.; Zhang, Y.; Yang, D.; Du, N. Scalable and low-cost synthesis of porous silicon nanoparticles as high-performance lithium-ion battery anode. *Mater. Today Nano* **2022**, *18*, 100175.
- (10) Waggoner, L. E.; Kang, J.; Zuidema, J. M.; Vijayakumar, S.; Hurtado, A. A.; Sailor, M. J.; Kwon, E. J. Porous silicon nanoparticles targeted to the extracellular matrix for therapeutic protein delivery in traumatic brain injury. *Bioconjugate Chem.* **2022**, 33 (9), 1685–1697.
- (11) Ge, M.; Rong, J.; Fang, X.; Zhang, A.; Lu, Y.; Zhou, C. Scalable preparation of porous silicon nanoparticles and their application for lithium-ion battery anodes. *Nano Res.* **2013**, *6*, 174–181.

- (12) Sailor, M. J. Porous Silicon in Practice: Preparation, Characterization and Applications; John Wiley & Sons, 2012.
- (13) Bimbo, L. M.; Sarparanta, M.; Santos, H. A.; Airaksinen, A. J.; Makila, E.; Laaksonen, T.; Peltonen, L.; Lehto, V.-P.; Hirvonen, J.; Salonen, J. Biocompatibility of thermally hydrocarbonized porous silicon nanoparticles and their biodistribution in rats. *ACS Nano* **2010**, *4* (6), 3023–3032.
- (14) Nissinen, T.; Ikonen, T.; Lama, M.; Riikonen, J.; Lehto, V.-P. Improved production efficiency of mesoporous silicon nanoparticles by pulsed electrochemical etching. *Powder Technol.* **2016**, 288, 360–365.
- (15) Russo, L.; Colangelo, F.; Cioffi, R.; Rea, I.; Stefano, L. D. A mechanochemical approach to porous silicon nanoparticles fabrication. *Materials* **2011**, *4* (6), 1023–1033.
- (16) Xu, W.; Rytkönen, J.; Rönkkö, S.; Nissinen, T.; Kinnunen, T.; Suvanto, M.; Närvänen, A.; Lehto, V.-P. A nanostopper approach to selectively engineer the surfaces of mesoporous silicon. *Chem. Mater.* **2014**, 26 (23), 6734–6742.
- (17) Xu, W.; Thapa, R.; Liu, D.; Nissinen, T.; Granroth, S.; Narvanen, A.; Suvanto, M.; Santos, H. A.; Lehto, V.-P. Smart porous silicon nanoparticles with polymeric coatings for sequential combination therapy. *Mol. Pharmaceutics* **2015**, *12* (11), 4038–4047.
- (18) Tasciotti, E.; Liu, X.; Bhavane, R.; Plant, K.; Leonard, A. D.; Price, B. K.; Cheng, M. M.-C.; Decuzzi, P.; Tour, J. M.; Robertson, F.; et al. Mesoporous silicon particles as a multistage delivery system for imaging and therapeutic applications. *Nat. Nanotechnol.* **2008**, 3 (3), 151–157.
- (19) Chiappini, C.; Liu, X.; Fakhoury, J. R.; Ferrari, M. Biodegradable porous silicon barcode nanowires with defined geometry. *Adv. Funct. Mater.* **2010**, *20* (14), 2231–2239.
- (20) Heinrich, J. L.; Curtis, C. L.; Credo, G. M.; Sailor, M. J.; Kavanagh, K. L. Luminescent colloidal silicon suspensions from porous silicon. *Science* **1992**, 255 (5040), 66–68.
- (21) Qin, Z.; Joo, J.; Gu, L.; Sailor, M. J. Size control of porous silicon nanoparticles by electrochemical perforation etching. *Part. Part. Syst. Charact.* **2014**, *31* (2), 252–256.
- (22) Roberts, D. S.; Estrada, D.; Yagi, N.; Anglin, E. J.; Chan, N. A.; Sailor, M. J. Preparation of Photoluminescent Porous Silicon Nanoparticles by High-Pressure Microfluidization. *Part. Part. Syst. Charact.* **2017**, *34* (3), 1600326.
- (23) Santos, H. A.; Mäkilä, E.; Airaksinen, A. J.; Bimbo, L. M.; Hirvonen, J. Porous silicon nanoparticles for nanomedicine: preparation and biomedical applications. *Nanomedicine* **2014**, 9 (4), 535–554.
- (24) Asadi, A.; Pourfattah, F.; Miklós Szilágyi, I.; Afrand, M.; Żyła, G.; Seon Ahn, H.; Wongwises, S.; Minh Nguyen, H.; Arabkoohsar, A.; Mahian, O. Effect of sonication characteristics on stability, thermophysical properties, and heat transfer of nanofluids: A comprehensive review. *Ultrason. Sonochem.* **2019**, *58*, 104701.
- (25) Ali, F.; Reinert, L.; Levêque, J. M.; Duclaux, L.; Muller, F.; Saeed, S.; Shah, S. S. Effect of sonication conditions: solvent, time, temperature and reactor type on the preparation of micron sized vermiculite particles. *Ultrason. Sonochem.* **2014**, *21* (3), 1002–1009.
- (26) Show, K.-Y.; Mao, T.; Lee, D.-J. Optimisation of sludge disruption by sonication. *Water Res.* **2007**, *41* (20), 4741–4747.
- (27) Dove, P. M.; Craven, C. M. Surface charge density on silica in alkali and alkaline earth chloride electrolyte solutions. *Geochim. Cosmochim. Acta* **2005**, *69* (21), 4963–4970.
- (28) Alvarez-Berrios, M. P.; Aponte-Reyes, L. M.; Aponte-Cruz, L. M.; Loman-Cortes, P.; Vivero-Escoto, J. L. Effect of the surface charge of silica nanoparticles on oil recovery: wettability alteration of sandstone cores and imbibition experiments. *Int. Nano Lett.* **2018**, *8*, 181–188.
- (29) Kurhekar, A. S.; Apte, P. R. Spectroscopic-ellipsometric study of native oxide removal by liquid phase HF process. *Int. Nano Lett.* **2013**, *3*, 10.
- (30) Rodríguez Durán, I.; Durocher-Jean, A.; Profili, J.; Stafford, L.; Laroche, G. Atmospheric pressure Townsend discharges as a promising tool for the one-step deposition of antifogging coatings

ı

- from N2O/TMCTS mixtures. Plasma Processes Polym. 2020, 17 (7), 1900186.
- (31) Sillars, D.; Bennett, C. J.; Osamura, Y.; Kaiser, R. I. First infrared spectroscopic characterization of the disilyl (Si2HS) and dS-disilyl (Si2DS) radicals in low temperature silane matrices. *Chem. Phys.* **2004**, *305* (1–3), 141–153.
- (32) Ellerbrock, R.; Stein, M.; Schaller, J. Comparing amorphous silica, short-range-ordered silicates and silicic acid species by FTIR. Sci. Rep. 2022, 12 (1), 11708.
- (33) Brunauer, S.; Emmett, P. H.; Teller, E. Adsorption of gases in multimolecular layers. *J. Am. Chem. Soc.* **1938**, *60* (2), 309–319.
- (34) Vaccari, L.; Canton, D.; Zaffaroni, N.; Villa, R.; Tormen, M.; di Fabrizio, E. Porous silicon as drug carrier for controlled delivery of doxorubicin anticancer agent. *Microelectron. Eng.* **2006**, *83* (4–9), 1598–1601.
- (35) Wu, E. C.; Park, J.-H.; Park, J.; Segal, E.; Cunin, F.; Sailor, M. J. Oxidation-triggered release of fluorescent molecules or drugs from mesoporous Si microparticles. *ACS Nano* **2008**, *2* (11), 2401–2409.
- (36) Gu, L.; Park, J. H.; Duong, K. H.; Ruoslahti, E.; Sailor, M. J. Magnetic luminescent porous silicon microparticles for localized delivery of molecular drug payloads. *Small* **2010**, *6* (22), 2546–2552.
- (37) Wu, E. C.; Andrew, J. S.; Buyanin, A.; Kinsella, J. M.; Sailor, M. J. Suitability of porous silicon microparticles for the long-term delivery of redox-active therapeutics. *Chem. Commun.* **2011**, 47 (20), 5699–5701
- (38) Wu, E. C.; Andrew, J. S.; Cheng, L.; Freeman, W. R.; Pearson, L.; Sailor, M. J. Real-time monitoring of sustained drug release using the optical properties of porous silicon photonic crystal particles. *Biomaterials* **2011**, 32 (7), 1957–1966.
- (39) Nan, K.; Ma, F.; Hou, H.; Freeman, W. R.; Sailor, M. J.; Cheng, L. Porous silicon oxide-PLGA composite microspheres for sustained ocular delivery of daunorubicin. *Acta Biomater.* **2014**, *10* (8), 3505–3512.
- (40) Pérez, K. S.; Warther, D.; Calixto, M. E.; Méndez-Blas, A.; Sailor, M. J. Harnessing the Aqueous Chemistry of Silicon: Self-Assembling Porous Silicon/Silica Microribbons. *ACS Appl. Mater. Interfaces* **2019**, *11* (30), 27162–27169.
- (41) Dorvee, J. R.; Derfus, A. M.; Bhatia, S. N.; Sailor, M. J. Manipulation of liquid droplets using amphiphilic, magnetic one-dimensional photonic crystal chaperones. *Nat. Mater.* **2004**, 3 (12), 896–899.
- (42) Zhou, J.; Huang, X.; Lan, D.; Cheng, Y.; Xue, F.; Jia, C.; Wu, G.; Jia, Z. Polymorphic cerium-based Prussian blue derivatives with in situ growing CNT/Co heterojunctions for enhanced microwave absorption via polarization and magnetization. *Nano Res.* **2023**, *17*, 2050–2060.
- (43) Bertucci, A.; Kim, K.-H.; Kang, J.; Zuidema, J. M.; Lee, S. H.; Kwon, E. J.; Kim, D.; Howell, S. B.; Ricci, F.; Ruoslahti, E.; et al. Tumor-targeting, microRNA-silencing porous silicon nanoparticles for ovarian cancer therapy. *ACS Appl. Mater. Interfaces* **2019**, *11* (27), 23926–23937.
- (44) Gongalsky, M. B.; Kargina, J. V.; Cruz, J. F.; Sánchez-Royo, J. F.; Chirvony, V. S.; Osminkina, L. A.; Sailor, M. J. Formation of Si/SiO2 luminescent quantum dots from mesoporous silicon by sodium tetraborate/citric acid oxidation treatment. *Front. Chem.* **2019**, *7*, 165.
- (45) Bansal, R.; Singh, R.; Kaur, K. Quantitative analysis of doxorubicin hydrochloride and arterolane maleate by mid IR spectroscopy using transmission and reflectance modes. *BMC Chem.* **2021**, *15* (1), 27.